Metal-ligand cooperative activation of HX (X=H, Br, OR) bond on Mn based pincer complexes

Krieger, Annika M.; Sinha, Vivek; Kalikadien, Adarsh V.; Pidko, Evgeny A.

DOI
10.1002/zaac.202100078

Publication date
2021

Document Version
Final published version

Published in
Zeitschrift fur Anorganische und Allgemeine Chemie

Journal of Inorganic and General Chemistry
ZAAC
Zeitschrift für anorganische und allgemeine Chemie
DOI: 10.1002/zaac.202100078
ARTICLE

Metal-ligand cooperative activation of HX (X = H, Br, OR) bond on Mn based pincer complexes

Annika M. Krieger,[a] Vivek Sinha,*[a] Adarsh V. Kalikadien,[a] and Evgeny A. Pidko*[a]

Reversible dissociation of H–X bond (M–L + H–X→M(X)-L(H); ΔG_{HX}) is an important step during pre-activation, catalysis and possible deactivation of acid-base cooperative pincer based transition metal catalysts (M–L). Herein we carried out a high-throughput computational investigation of the thermodynamic stability of different adducts in various functionalized Mn(I) based pincer complexes. We used a combination of density functional theory (DFT) and density functional tight binding (DFTB) calculations to analyze ΔG_{HX} of >700 (M(X)-L(H)) intermediates based on functionalized variants of four pincer type ligand scaffolds derived from PCP, CNC, PNP and SNS ligands. We discovered linear scaling relations between ΔG_{HX} of various species. Strongest correlations were found between species of similar size and chemical nature e.g. ΔG_{tBuOH} correlated best with ΔG_{iPrOH} and worst with ΔG_{HBr}. Such scaling relations can be useful for property based screening of catalysts and selection of (co)solvent/substrate/base for optimized reaction conditions. We also investigated the influence of the ligand backbone and the functionalization of donor and backbone sites in the ligand. Our analysis reveals the crucial role of the second coordination sphere functionalization for the reactivity of the complexes with impact in some cases exceeding that of the variation of the functional groups directly attached to the donor atoms.

Introduction

Pincer complexes are important catalysts in organometallic chemistry for multiple applications such as transformation and synthesis of imines, amines, peptides, pyridines, pyrroles, acetals, and carboxylic acid derivatives, such as esters, ketones and amides.[1–3] Owing to their success with (de)hydrogenation of a wide scope of substrates, pincer complexes have been adopted favorably by the pharmaceutical, fine chemicals and the energy industry[4] (representative examples shown in Figure 1a,b). The well-defined geometry and tridentate coordination mode of this class of complexes offers a stable catalytic structure. Most highly active pincers such as Ru-MACHO complex[5,6] and Nozaki's Ir-PNP complex[7] are based on expensive Ru and Ir metals. Catalytic systems based on such metals are not desirable for large scale ubiquitous applications due to high cost and limited availability. Several successful examples of pincer catalysts based on earth abundant 3d transition metals (TMs) such as Fe and Mn have been realized in the last decade.[8,9] However, the activity and stability of such catalysts based on first row TMs remains a challenge. Therefore, the development and optimization of catalysts based on 3d transition metals is an active and highly sought after area of research.[10–12] Manganese is particularly attractive as the active metal in such catalysts in view of its high biocompatibility, which is of interest for industries in the food or pharmaceutical sector.

Functionalization of the ligand scaffold can be used to explore the chemical space of TM pincers in the pursuit of highly active and stable catalysts based on first row TMs. In such an approach one can start with a "skeleton" complex bearing a TM center coordinated to a pincer scaffold. Selected sites on the scaffold or metal center can be functionalized generating an ensemble of new TM complexes using various combinations of functional groups.[13–16] Experimentally only a handful of functionalized variants of pincer ligand scaffolds have been reported. Moreover, synthesis and subsequent testing of the catalytic activity of functionalized TM complexes quickly becomes intractable. Theoretical consideration of the functionalized variants that are synthetically not accessible can provide an insight into rational design principles. In this regard, computational methods are relevant and can be applied to screen through a large ensembles of functionalized TM complexes.[17,18] Recently such approaches have been applied to screen TM complex including pincer complexes for activity, regioselectivity and ligand effects.[19–21]

Herein we screened the effect of functionalization of the ligand backbone on the stability of potential catalytic intermediates on Mn(I)-pincer complexes. The focus was on the determination of the effect of the type of functionalization and the functionalization site (backbone/donor site). By choosing functionalization sites directly coordinated to the Mn(I)-center, the effect of the first coordination sphere can be analyzed. The effect of the second coordination sphere is rationalized by

[a] A. M. Krieger, Dr. V. Sinha, A. V. Kalikadien, Prof. Dr. E. A. Pidko
Inorganic Systems Engineering, Department of Chemical Engineering, Faculty of Applied Sciences, Delft University of Technology, van der Maasweg 9, 2629 HZ, Delft, The Netherlands
E-mail: V.Sinha@tudelft.nl
E.A.Pidko@tudelft.nl

Supporting information for this article is available on the WWW under https://doi.org/10.1002/zaac.202100078 and https://doi.org/10.4121/14571984.v1

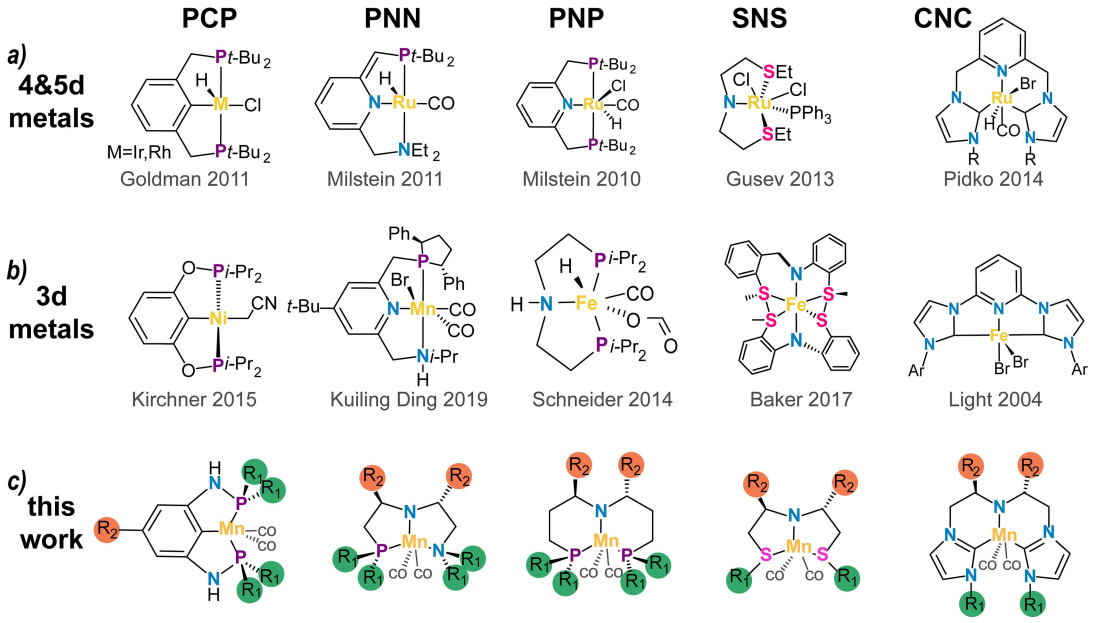

Figure 1. Representative transition metal pincer complexes of (a) 4d, 5d and (b) 3d metals, followed by (c) the catalyst scope of this work.

investigating functionalization on a site not directly coordinated to the metal. We chose five representative pincer ligand scaffolds, namely, PNP- (bis(3-phosphaneylpropyl)amine)-, SNS- (azanediylbis(ethane-1-thiol))-, CNC- (bis(2-(1H-3λ^4-imidazol-3-yl) ethyl)amine)-, PNN- (N^1-(2-phosphaneylethyl)ethane-1,2-diamine)-, and PCP- (N^1,N^3-bis(phosphaneyl)benzene-1,3-diamine)-backbones coordinated to a Mn(I) center stabilized by CO ligands as illustrated in Figure 1c. Our analysis included the pristine complexes as well as their catalytically relevant intermediates resulting in over ~1200 structures based on the five selected pincer ligand scaffolds (Figure 1c).

Pincer complexes based on these ligands have been reported for various transition metals, including manganese (Figure 1b).[8,13,30,31,22–29] SNS-,[32–37] CNC-,[38–43] and PCP-ligands[44–48] are primarily known for their use in 4d and 5d transition metal catalysis (Figure 1a). Especially in 4d and 5d-transition metal catalysis high turnover frequencies and turnover numbers are reported for the complexes.[31,40,42,49]

Literature on 3d-transition metals generally reports lower catalytic efficiencies,[30,48] which indicates that there is opportunity to maximize their potential towards sustainable catalyst systems. Catalysts based on 3d metals are known to be more prone to deactivation and formation of resting states, limiting their reactivity.[4,50]

Herein, we investigated Mn(I) -pincers as potential (de) hydrogenation catalysts. Possible applications are the storage of H_2 in unsaturated moieties such as CO_2, the reduction of organic substrates with H_2 gas or with hydrogen donors such as *i*-PrOH.[51–53] Figure 2 illustrates representative catalytic cycles of dehydrogenation of methanol to formaldehyde and hydrogenation of acetone to isopropanol. The Br adduct (M(Br)–L(H)) is a common precursor to the active form of Mn-pincers.[11] The activation of the catalyst is commonly carried out by the

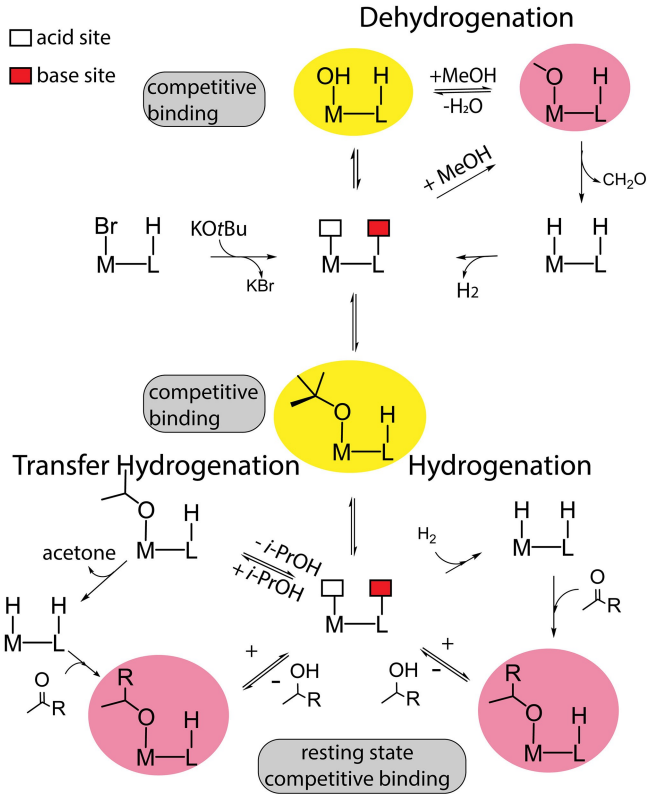

Figure 2. Representative catalytic cycles for dehydrogenation and hydrogenation reactions with possible competing and deactivation pathways. Dehydrogenation of methanol in aqueous phase and hydrogenation of acetone to *i*-PrOH have been used as representative examples. Possible alkoxides and hydroxide based competing and resting states have been highlighted in yellow and red respectively.

reaction with a strong base (e.g. KOH or KO*t*-Bu). This yields a 5-coordinated complex (M–L), regarded as a pristine activated catalyst and which features a Lewis acid site on the metal and the ligand can act as a Brønsted base i.e. the metal can coordinate with an electron donating species while the ligand can accept a H^+. The activated catalyst is susceptible for potential deactivation/inhibition through the metal-ligand co-operative addition of alcohol/water/base resulting in the formation of –OR adducts.[54] Alkoxide adduct of hydrogen donating alcohols such *i*-PrOH, MeOH and EtOH are often formed as intermediates in the course of catalytic hydrogenation reactions, and can even act as the resting states limiting the catalytic performance depending on their stability.[50,55–60] Competitive bonding of other species such as the solvent or the nucleophile base to the metal can slow down or even deactivate the catalyst.

For example, water can compete with methanol for the catalytically active site via the formation of a stable hydroxide adduct upon reaction with the catalyst or via ligand exchange with the methoxide adduct (Figure 2). To continue the catalytic cycle, the alkoxide adduct must convert to the hydride adduct (M(H)-L(H)), which in turn regenerates the catalyst by hydrogen evolution/transfer. Catalytic turnover is inhibited if the alkoxide adduct is very stable compared to the hydride adduct. Similarly, an excessively stable hydride adduct would render it inactive towards hydrogen liberation resulting in an adverse effect on the catalysis.

When employed as a hydrogenation catalyst, the hydride adduct is formed in the first step via heterolytic H_2 dissociation. A less stable hydride would be prone to H_2 recombination instead of catalytic turnover. On the other hand, excessive hydride stability would make it less reactive towards the hydride transfer steps of the catalytic cycle. The alkoxide adduct formed upon the hydride transfer to C=O must dissociate to regenerate the catalyst.

Transfer hydrogenation reactions with e.g. isopropanol often proceeds via the formation of an intermediate alkoxide species. Excessive stability of this alkoxide adduct would have a deactivating effect and adversely affect the catalytic turnover. From a mechanistic perspective the relative stability of hydride, hydroxide and alkoxide intermediates are important for the catalytic turnover. Their relative stability, in accordance with the Sabatier's principle should be balanced and any excessive stabilization/destabilization would have an inhibiting effect on the catalyst.

In the present work we investigate functional strategies to tune the stability of aforementioned intermediates. Our results allow comparison of different ligand scaffolds and functionalization strategies in a common framework. We have identified linear free energy scaling relations (LFESRs) between various intermediates. By analyzing relative stabilities of various adducts we analyze their competitive binding at the metal center. We describe the impact of functionalization of the complexes near the metal center and on the ligand backbone. Finally, we draw conclusions about catalyst behavior and formulate perspectives on catalyst activation strategies, choice of solvent environment and possible deactivation species. The paper is organized as follows: in the computational methods section we describe the functionalization approach, computational model to investigate the thermodynamic parameters, and details of the quantum chemical calculations applied. Next we describe and discuss the results from our calculations. Finally we summarize the results and present our conclusions.

Computational methods

Electronic structure calculations on the transition metal complexes were carried out either by using the extended density functional tight-binding (DFTB) or the density functional theory (DFT) methods. For a large number of calculations, a full DFT based approach is computationally expensive. Extended DFTB calculations via the xTB code from Grimme's group has recently emerged as a rapid tool with reasonable accuracy to predict geometry and thermochemistry of various chemical systems including TM complexes.[61] We therefore performed xTB calculations on all the complexes in our paper. On a selected number of TM complexes (432) based on CNC, PCP and PNN ligands, we also performed DFT calculations. xTB calculations on the same 432 complexes were compared with DFT based predictions to determine the accuracy of xTB.

Extended density functional tight-binding calculations

Extended DFTB calculations were performed using the xTB software suite (version 6.3.3).[62,63] The GFN2-xTB method was applied for geometry optimization, using the *verytight* criteria. Hessian matrix calculations were performed for all optimized geometries to verify the absence of imaginary frequencies and that each geometry corresponds to a local minimum on its respective potential energy surface (PES). The GBSA solvation model parametrized for THF as implemented in xTB was used to account for solvent effects.

Density functional theory calculations

Density functional theory (DFT) calculations were performed using the Gaussian 16 C.01 suite of software.[64] All geometries were optimized using the BP86 functional with a def2-SVP basis set in the gas phase.[65] This combination of functional and basis set gives reliable geometry predictions accompanied with low computational costs.[66,67] Hessian calculations were performed to ensure that all optimized geometries were a minima on the PES (no imaginary mode). Zero-point energy and Gibbs free energy corrections to electronic energy were obtained from hessian calculations within the harmonic approximation under standard conditions (298.15 K, 1 bar). Single point (SP) energy calculations with the SMD[68] solvation (THF) model were carried out using the PBE0 hybrid functionals[69] with a triple zeta basis set (def2-TZVP) to further refine the electronic energies. SPs were also carried out using the BP86 functional.[70] We denote such composite methods BP86/def2-SVP//XC/def2-TZVP (THF),

as bp86(thf) or pbe0(thf) depending on the exchange-correlation (XC) functional used for the SP single-point calculations. This allowed to investigate the impact of solvation (bp86(gas) vs bp86(THF)) and the functional (bp86(THF) vs pbe0(THF)) on the computed free energies. All DFT calculations were performed with dispersion correction (D3).[71]

DFT calculations were performed for a selected number of complexes bearing CNC, PNN and PCP ligands. We focused our investigation on the addition of H–X species (X = H, OH, MeO, EtO, *i*-PrO, *t*-BuO, Br) across the catalyst which is represented as M–L, where M represents the metal center and L represents the ligand. Addition of H–X across M–L leads to formation of M(X)–L(H) species, where metal forms an adduct with X and the ligand gets protonated. We estimated the thermodynamic stability of M(X)–L(H) by computing the Gibbs free energy change under standard conditions upon addition of H–X moiety across M–L bond (eq. (1)).

$$H-X+M-L \rightarrow M(X)-L(H)$$
$$\Delta G^{\circ}_{HX} = G(M(X)-L(H)) - G(M-L) - G(H-X) \quad (1)$$

Results and Discussion

Functionalization strategy

All functionalized geometries were obtained via an *in-house* developed automated python based workflow.[72] We chose two different functionalization sites: four R_1 sites which are located near the metal center, and two R_2 sites (only one in case of PCP) which functionalize the ligand backbone as shown in Figure 1. We chose to perform symmetric functionalizations meaning all four R_1 sites were kept the same, and both R_2 sites were also functionalized with the same ligand. R_1 and R_2 were however not constrained to be the same. In addition to functionalization sites on the ligand, seven Mn-adducts were also considered which included vacant site (pristine complex), H, Br, MeO, *i*-PrO, EtO and *t*-BuO adducts. This functionalization scheme generated ~1200 geometries of metal complexes. Out of these 1225 geometries, we filtered geometries where the pristine complex had a hemi-labile ligand resulting in a total of 732 geometries which are discussed in this work. We found that most PNN based complexes resulted in hemi-labile ligand. Hemi-lability can arise as an artifact of xTB based geometry optimization or it can be genuinely present in the system. Since this would require further investigation we excluded all xTB based results for the PNN catalyst.

Comparison of xTB with DFT

Low computational cost and wide applicability of xTB calculations make them suitable for high throughput screening of TM complexes. The accuracy of xTB calculations has not been tested for Mn complexes. To investigate the accuracy of xTB calculations with respect to DFT based results, we computed CO stretching frequencies and ΔG_{HX} for selected complexes. Figure 3 compares xTB and DFT results for addition of HBr to

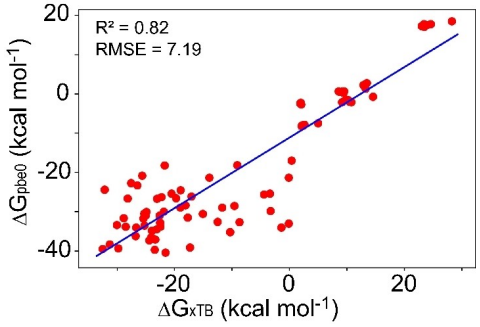

Figure 3. Correlation between Gibbs free energies for addition of HBr computed using xTB (x-axis) and DFT (y-axis).

Mn-PCP, Mn-PNN and Mn–CNC complexes. DFT and xTB computed ΔG_{HBr} agree well with $R^2 = 0.82$ and a RMSE (based on the linear fit; see SI) of 7.19 kcal mol^{-1}. The correlation coefficient between xTB and DFT computed ΔG_{iPrOH} is relatively poor ($R^2 = 0.28$; RMSE = 10.48 kcal mol^{-1}) and the two methods reach only qualitative agreement (see SI) for the addition of *i*-PrOH.

To further compare the performance of xTB and DFT, we analyzed the computed CO stretching frequencies (ν(CO)) for the carbonyl moieties in the Mn pincers. A comparison of the results obtained with the DFT and xTB methods for a representative case of Mn-PCP complex is presented in Figure 4. Both methodologies reveal a similar trend in computed ν(CO). For a given R_1, electron donating R_2 groups give rise to lower ν(CO). The plots also show that the electron donating effect of R_1 functionalziation in this case is more important that that of the R_2, because of the major role of the electronic effects at the metal center on the coordinated CO ligands. Furthermore, we observed a good agreement between xTB and DFT results when all systems with CF_3 functionalization are excluded from the dataset ($R^2 = 0.85$). xTB calculations seem to overestimate the CO stretching for CF_3 functionalized ligands for all pincer complexes considered in this study (see SI). Nevertheless, the comparison of ΔG_{HX} and ν(CO) parameters point to a qualitative agreemenet between the results obtained with the xTB and DFT methods.

Scaling Relations and competitive adduct formation

The activation of H–X bonds is assumed to proceed via a metal-ligand cooperative heterolytic cleavage over the M–L site in all of the pincer complexes discussed here. We therefore, expect similar trends in Gibbs free energy for addition of H–X species, with differences arising from the nature of M–X bonding. Such similarities practically manifest themselves in scaling or linear free energy relationships between different substrates. Such relationships imply that having computed the ΔG_{HX_1} for a substrate HX_1, one can estimate the ΔG_{HX_i} for all other species that follow a linear scaling relation with HX_1. Figure 5 shows a significant correlation between the DFT-computed ΔG_{HBr} and

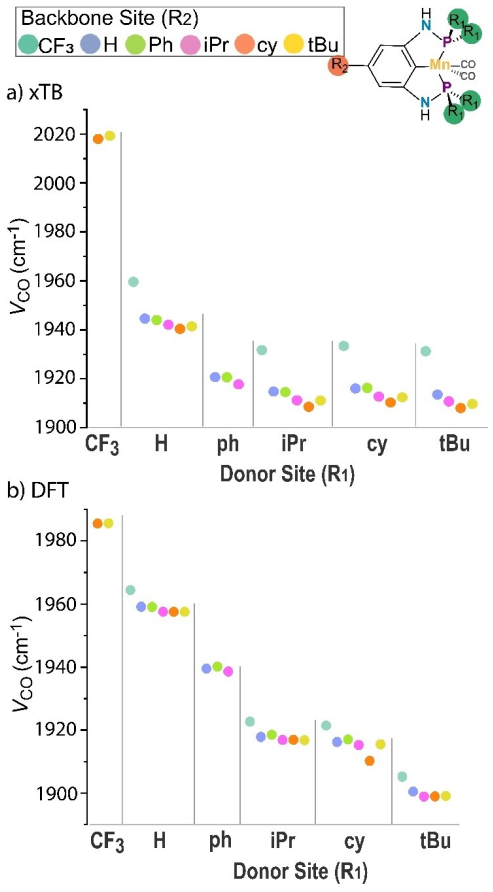

Figure 4. a) xTB and b) DFT computed ν(CO) for Mn–PCP complexes sorted by electron donating properties of the functionalization group.

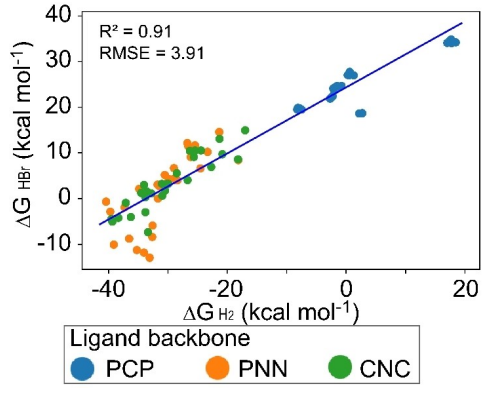

Figure 5. Comparison DFT computed Gibbs free energy of formation of bromide and hydride adducts in Mn–PCP, Mn-PNN and Mn–CNC complexes.

ΔG_{H2} using DFT ($R^2 = 0.91$), especially for PCP and CNC complexes. Therefore, the Gibbs free energy of the bromide adduct formation can be used to estimate the relative energy of formation of the hydride species.

In our experience metal hydride complexes are not described well using xTB.[73] Often the M–H bond was found to be very elongated (>2.8 Å) (see SI) in the structures obtained by the xTB-based geometry optimizations. However, Br complexes are described well and reasonable geometries were obtained with both xTB and DFT optimizations. Therefore, the scaling relationship that we observed between the bromide and hydride adduct becomes particularly practical because the ΔG_{HBr} computed using xTB can be directly used to estimate the stability of the active hydride intermediates in screening studies.

Figure 5 also shows that while both PCP and PNN complexes react with H_2 in an exergonic manner, the reaction is endergonic with Mn–CNC complexes. DFT calculations also revealed linear scaling relations among hydride, iso-propoxide, bromide and hydroxide adducts. The correlation of ΔG_{H_2} with OH and *i*-PrO adduct was found to be rather weak ($R^2 = 0.53$ and 0.55) (see SI). We attribute this weaker correlation to differences in M–X bonds formed upon addition of H–X (M–OR vs. M–H) (*vide infra*). ΔG_{H_2O} and ΔG_{iPrOH} were found to have a moderate correlation with $R^2 = 0.71$. We also investigated the correlation coefficient between the xTB-computed ΔG_{HX} values. The resulting correlation matrix is shown in Figure 6. We observe that Gibbs free energies for addition of chemically similar species have higher correlation coefficient. For example, all alkoxides correlate well among each other but have relatively poor correlation with hydrides and bromides. Therefore, isopropoxide and ethoxide have the strongest correlation followed by the correlation between methoxide and ethoxide. The weakest correlation is between the Mn-alkoxides and the catalyst precursor (Mn–Br).

Adduct stability modulations via ligand modifications

Next we investigated the impact of the functionalization of donor site vs backbone on ΔG_{HX}. For this purpose we examined ΔG_{HBr} in two scenarios: 1) $R_2 = H$ with R_1 varied to investigate the impact of functionalization at the donor site 2) $R_1 = H$ with R_2 varied to investigate the impact of functionalization on the ligand backbone. Functionalizations on the ligand either on donor or acceptor site can have a stabilizing or a destabilizing

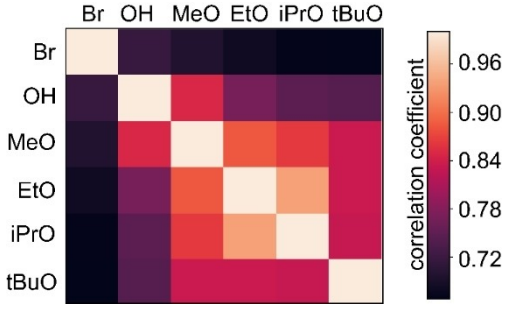

Figure 6. Correlation matrix of Gibbs free energy of formation in all ligand backbones investigated by xTB for different metal adducts.

effect in two ways: 1) via (de)stabilization of the pristine catalyst 2) Electronic and/or steric (de)stabilization of the adduct moieties. The pristine complex can be (de)stabilized via geometric distortions and the resulting strain in the ligand scaffold introduced by functionalization. The adduct moiety such as an alkoxide can be destabilized by increased electronic density at the metal center. On the other hand, the L–H bond in the adducts can be favorably stabilized by an increased electronic density at the ligand. Larger alkyl groups such as *t*-Bu/cy can also destabilize bulky alkoxides by steric repulsion. An accurate consideration of electronic effects is necessary to examine the impact of functionalization. Therefore we examined the impact of functionalization of ΔG_{HX} using DFT calculations.

Functionalization on donor site

R_2 = H resulted in five PCP (R_1 = H, Ph, *i*-Pr, cy, *t*-Bu), four CNC (R_1 = CF_3, Ph, *i*-Pr and cy) and three PNN (R_1 = Ph, *i*-Pr and *t*-Bu) ligand complexes. The resulting $\Delta G_{HX}$are presented in Table S5. For both PCP and PNN complexes, electron donating groups at R_1 destabilize the adduct leading to higher (more positive) ΔG_{HX}. In contrast to PCP and PNN complexes, the CNC complexes exhibit a different trend. The electron withdrawing CF_3 groups also destabilize Br and OH adducts. A detailed analysis of this divergent trend is beyond the scope of this paper. We speculate that these differences are related to the nature of Mn–C coordination in the CNC complexes. Furthermore, the R_1 functionalizations in this case are not performed on the C moiety coordinating the Mn center unlike for the other complexes where the functionalized P/N/S are directly bound with the metal site.

Functionalization on ligand backbone

Primarily two factors control the impact of functionalization on the ligand backbone: 1) electronic effect which influences the basicity of the acceptor site and 2) strain in the geometry upon functionalization. Electron releasing groups should increase the basicity of the acceptor site and, therefore, are expected to have a stabilizing effect. At the same, since electron releasing groups such as a *t*-Bu are bulkier they are also expected to introduce a high amount of strain in the coordinated ligand geometry. R_1 = *i*-Pr resulted in 6 CPC and PNN, and 5 PCP complexes with Br coordinated to the Mn. The resulting ΔG_{HBr} are presented in Table S7.

Variation of R_2 seems to have minimal impact on the PCP scaffold where ΔG_{HBr} shows little variation with the R_2 = H being the most stable complex, and R_2 = CF_3 being the least stable. This behavior is expected since the R_2 site is located further away from the proton acceptor site on the ligand. For both Mn-PNN and Mn–CNC complexes, R_2 = cy results in most favorable adduct formation. R_2 = CF_3 leads to most destabilized adduct for the Mn–CNC, whereas R_2 = *t*-Bu is most destabilizing functionalization for Mn-PNN. The additional stabilization of *cy* substitution is in contrast with the destabilization introduced by other electron donating groups namely Ph, *i*-Pr and *t*-Bu. The Hamett constants of cy and *i*-Pr are −0.05 and −0.04, respectively, indicating similar electron releasing behavior via inductive effect.[74] We attribute the observed destabilizing effect of Ph, *i*-Pr and *t*-Bu groups, despite their electron donating nature, to the geometric strain. Analysis of geometric strain showed that R_2 = cy scaffold had an effective stabilization of 4.15 kcal mol^{-1} relative to R_2 = H. In contrast while R_2 = *i*-Pr suffered a destabilization of 1.37 kcal mol^{-1} (Table S5–S6). Therefore both steric and inductive effects play an important role in stabilization of the Br adducts.

Heatmap plots for the functionalization on donor and ligand backbone sites respectively represent the average impact of the choice of the functionalization groups (Figure S9). Both donor and backbone site functionalization leads to a great spread in average Gibbs free energy of formation, which can vary by up to 20 kcal mol^{-1} between different functionalizations. This reflects the degree of tunability of the catalytic properties that these ligand scaffolds can offer. Especially interesting are the qualitative changes in the average stability, where for example the substitution of CF_3 on the backbone site can turn the adduct formation from exergonic to endergonic. The relative range and standard deviation does not change significantly within the data sets.

Catalytic adduct species

With regards to the catalytic cycle, different adduct stabilities that play a significant role in activity and efficiency are examined. The heatmaps of the average formation Gibbs free energies show the difference between the investigated adducts (Figure S9). The results indicate that the bromide adduct sustains substantial stability upon functionalization, especially for CNC complexes. The stabilities of the other adducts with similar structure such as MeO and EtO, or *t*-BuO and *i*-PrO are quite similar.

Boxplots comparing the difference formation Gibbs free energies for the catalysts with different ligands are shown in Figure 7 and 8 allow to analyze the trends in more detail. One interesting aspect in (de)hydrogenation chemistry is the choice of the base activator/promotor for the catalytic reaction. An enhanced stability of a complex formed with the base can result in inhibition and the catalyst can remain in a resting state. Here, we considered a model (de)hydrogenation of *i*-PrOH reaction as an example.

In Figure 7 and 8, the stability of isopropxide to the adduct of two potential bases (KOH and KO*t*Bu, respectively) is compared. The results show that a competition between the base (KO*t*Bu) and *i*-PrOH for complexation with the Mn center is highly likely. However, the *i*-PrO adduct was generally found to be more stable than the OH adduct for all Mn-pincers studied here. This concludes that KOH may represent a better choice for the systems where *i*-PrOH dehydrogenation is important. Consistent with our observation, Beller and co-workers observed that switching from KOH to KO*t*Bu lead to catalyst

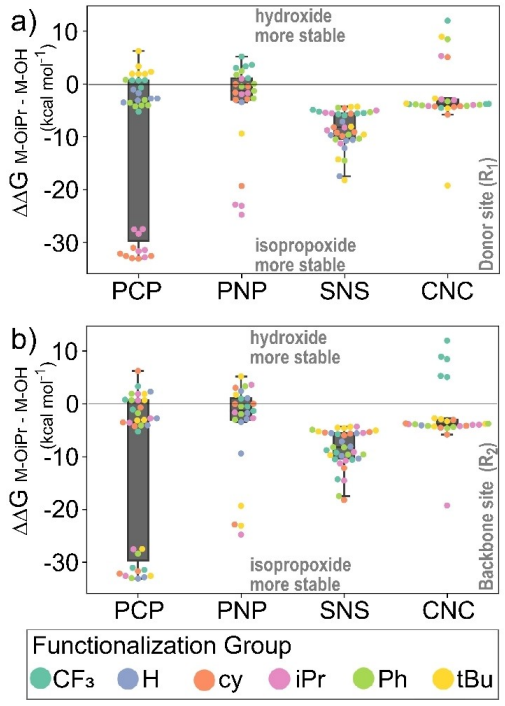

Figure 7. Comparison of isopropxide stabilities with hydroxide per catalytic ligand group. Swarmplots are added to indicate the functionalization on a) catalyst donor site R_1 and b) catalyst backbone site R_2.

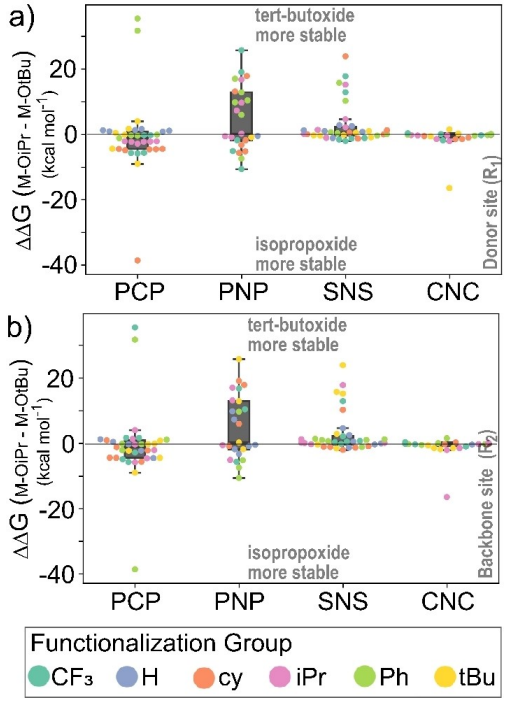

Figure 8. Comparison of isopropxide stabilities with tert-butoxide per catalytic ligand group. Swarmplots are added to indicate the functionalization on a) catalyst donor site R_1 and b) catalyst backbone site R_2.

deactivation in dehydrogenation of methanol catalyzed by a Mn-PNP pincer complex.[54]

Conclusions

In this investigation, we carried out a computational analysis of the effect of functionalization on different Mn-adducts of five types of pincer catalysts. Here, a data augmented approach was employed using fast xTB optimizations to analyze stabilities of metal adducts that can play a significant role in the catalytic cycle. The xTB results were compared to DFT calculations, which showed qualitative agreement and helped identifying the accuracy boundary of the accelerated xTB methodologies for studying Mn(I)-pincer complexes. We identified linear scaling relation between Gibbs free energy for formation of different adducts, which can be used for rapid screening purposes.

Functionalization of the donor site directly affects the metal center activation, as illustrated by the changes in the computed CO stretching frequencies. Increased electronic density at the metal center and geometric strain both have destabilizing effects on the formation of alkoxide, hydroxide, bromide and hydride adducts. Comparison of relative stabilities of the isopropoxide adduct with hydroxide and tert-butoxide adducts showed that KO*t*Bu can have a poisoning effect during *i*-PrOH dehydrogenation, and that KOH would be a more suitable base.

In the outlook, this work is a first step in mechanism based high throughput screening of pincer ligand based catalysts. Development of data-augmented approaches to screen and design highly active homogeneous catalysts is an ongoing effort in our laboratory.

Author contributions

A. K. carried out calculations and analysed the results. V. S. conceived and supervised the project. A. V. K. generated functionalized geometries of pincer complexes, coordinated in carrying out xTB and DFT calculations and compiling datasets from calculations. E. A. P. played a supervisory role and directed the project. All the authors discussed the results and wrote the manuscript.

Acknowledgements

V. S. acknowledge the ARC-CBBC project 2016.008 for funding. A.K. and E.A.P. acknowledge the financial support from the European Research Council (ERC) under the European Union's Horizon 2020 Research and Innovation Programme (grant agreement no. 725686). The authors thank Mr. Rowin Borst for carrying out some of the xTB calculations. The use of supercomputer facilities was sponsored by NWO Domain Science. This work was primarily carried out on the Dutch national e-infrastructure with the support of SURF Cooperative. Part of the results were obtained using the DECI resource Kay based in Ireland at ICHEC with support from the PRACE.

Keywords: data-driven catalysis · linear scaling relations · catalyst design · (de)hydrogenation catalysis · catalyst deactivation

[1] S. Werkmeister, K. Junge, M. Beller, *Org. Process Res. Dev.* **2014**, *18*, 289–302.
[2] L. Maser, L. Vondung, R. Langer, *Polyhedron* **2018**, *143*, 28–42.
[3] S. Werkmeister, J. Neumann, K. Junge, M. Beller, *Chem. - A Eur. J.* **2015**, *21*, 12226–12250.
[4] P. A. Dub, J. C. Gordon, *Nat. Rev. Chem.* **2018**, *2*, 396–408.
[5] W. Kuriyama, T. Matsumoto, O. Ogata, Y. Ino, K. Aoki, S. Tanaka, K. Ishida, T. Kobayashi, N. Sayo, T. Saito, *Org. Process Res. Dev.* **2012**, *16*, 166–171.
[6] T. Otsuka, A. Ishii, P. A. Dub, T. Ikariya, *J. Am. Chem. Soc.* **2013**, *135*, 9600–9603.
[7] W. Aoki, N. Wattanavinin, S. Kusumoto, K. Nozaki, *Bull. Chem. Soc. Jpn.* **2016**, *89*, 113–124.
[8] M. Garbe, K. Junge, S. Walker, Z. Wei, H. Jiao, A. Spannenberg, S. Bachmann, M. Scalone, M. Beller, *Angew. Chemie Int. Ed.* **2017**, *56*, 11237–11241.
[9] F. Kallmeier, R. Kempe, *Angew. Chemie Int. Ed.* **2018**, *57*, 46–60.
[10] L. Alig, M. Fritz, S. Schneider, *Chem. Rev.* **2019**, *119*, 2681–2751.
[11] G. A. Filonenko, R. van Putten, E. J. M. Hensen, E. A. Pidko, *Chem. Soc. Rev.* **2018**, *47*, 1459–1483.
[12] F. Agbossou-Niedercorn, C. Michon, *Coord. Chem. Rev.* **2020**, *425*, 213523.
[13] a) E. A. Belinski, P. O. Lagaditis, Y. Zhang, B. Q. Mercado, C. Würtele, W. H. Bernskoetter, N. Hazari, S. Schneider, *J. Am. Chem. Soc.* **2014**, *136*, 10234–10237; b) S. Schneider, J. Meiners, B. Askevold, *Eur. J. Inorg. Chem.* **2012**, *2012*, 412–429.
[14] K. J. Evans, S. M. Mansell, *Chem. – A Eur. J.* **2020**, *26*, 5927–5941.
[15] A. J. Canty, A. Ariafard, G. Koten, *Chem. – A Eur. J.* **2020**, *26*, 15629–15635.
[16] G. D. Batema, M. Lutz, A. L. Spek, C. A. van Walree, G. P. M. van Klink, G. van Koten, *Dalt. Trans.* **2014**, *43*, 12200–12209.
[17] P. Friederich, G. dos Passos Gomes, R. De Bin, A. Aspuru-Guzik, D. Balcells, *Chem. Sci.* **2020**, *11*, 4584–4601.
[18] J. P. Janet, F. Liu, A. Nandy, C. Duan, T. Yang, S. Lin, H. J. Kulik, *Inorg. Chem.* **2019**, *58*, 10592–10606.
[19] M. D. Wodrich, B. Sawatlon, E. Solel, S. Kozuch, C. Corminboeuf, *ACS Catal.* **2019**, *9*, 5716–5725.
[20] B. Sawatlon, M. D. Wodrich, C. Corminboeuf, *Organometallics* **2018**, *37*, 4568–4575.
[21] M. D. Wodrich, M. Busch, C. Corminboeuf, *Helv. Chim. Acta* **2018**, *101*, e1800107.
[22] M. Glatz, B. Stöger, D. Himmelbauer, L. F. Veiros, K. Kirchner, *ACS Catal.* **2018**, *8*, 4009–4016.
[23] F. Bertini, M. Glatz, B. Stöger, M. Peruzzini, L. F. Veiros, K. Kirchner, L. Gonsalvi, *ACS Catal.* **2019**, *9*, 632–639.
[24] S. Kostera, M. Peruzzini, K. Kirchner, L. Gonsalvi, *ChemCatChem* **2020**, *12*, 4625–4631.
[25] L. Zhang, Z. Wang, Z. Han, K. Ding, *Angew. Chemie Int. Ed.* **2020**, *59*, 15565–15569.
[26] F. Ling, J. Chen, S. Nian, H. Hou, X. Yi, F. Wu, M. Xu, W. Zhong, *Synlett* **2020**, *31*, 285–289.
[27] A. Kumar, P. Daw, N. A. Espinosa-Jalapa, G. Leitus, L. J. W. Shimon, Y. Ben-David, D. Milstein, *Dalt. Trans.* **2019**, *48*, 14580–14584.
[28] L. Zhang, Y. Tang, Z. Han, K. Ding, *Angew. Chemie Int. Ed.* **2019**, *58*, 4973–4977.
[29] G. A. Filonenko, E. J. M. Hensen, E. A. Pidko, *Catal. Sci. Technol.* **2014**, *4*, 3474–3485.
[30] F. Schneck, M. Finger, M. Tromp, S. Schneider, *Chem. – A Eur. J.* **2017**, *23*, 33–37.
[31] a) J. Zhang, E. Balaraman, G. Leitus, D. Milstein, *Organometallics* **2011**, *30*, 5716–5724; b) B. Gnanaprakasam, J. Zhang, D. Milstein, *Angew. Chem.* **2010**, *122*, 1510–1513; *Angew. Chem. Int. Ed.* **2010**, *49*, 1468–1471.
[32] N. Biswas, R. Sharma, D. Srimani, *Adv. Synth. Catal.* **2020**, *362*, 2902–2910.
[33] J. Schörgenhumer, A. Zimmermann, M. Waser, *Org. Process Res. Dev.* **2018**, *22*, 862–870.
[34] X. Chen, Y. Jing, X. Yang, *Chem. – A Eur. J.* **2016**, *22*, 1950–1957.
[35] D. Spasyuk, S. Smith, D. G. Gusev, *Angew. Chemie Int. Ed.* **2013**, *52*, 2538–2542.
[36] T. Koizumi, T. Teratani, K. Okamoto, T. Yamamoto, Y. Shimoi, T. Kanbara, *Inorganica Chim. Acta* **2010**, *363*, 2474–2480.
[37] U. K. Das, S. L. Daifuku, T. E. Iannuzzi, S. I. Gorelsky, I. Korobkov, B. Gabidullin, M. L. Neidig, R. T. Baker, *Inorg. Chem.* **2017**, *56*, 13766–13776.
[38] X. Wu, L. Ji, Y. Ji, E. H. M. Elageed, G. Gao, *Catal. Commun.* **2016**, *85*, 57–60.
[39] M. Hernández-Juárez, J. López-Serrano, P. Lara, J. P. Morales-Cerón, M. Vaquero, E. Álvarez, V. Salazar, A. Suárez, *Chem. – A Eur. J.* **2015**, *21*, 7540–7555.
[40] G. A. Filonenko, E. Cosimi, L. Lefort, M. P. Conley, C. Copéret, M. Lutz, E. J. M. Hensen, E. A. Pidko, *ACS Catal.* **2014**, *4*, 2667–2671.
[41] A. R. Naziruddin, C.-L. Kuo, W.-J. Lin, W.-H. Lo, C.-S. Lee, B.-J. Sun, A. H. H. Chang, W.-S. Hwang, *Organometallics* **2014**, *33*, 2575–2582.
[42] S. Gründemann, M. Albrecht, J. A. Loch, J. W. Faller, R. H. Crabtree, *Organometallics* **2001**, *20*, 5485–5488.
[43] A. A. Danopoulos, N. Tsoureas, J. A. Wright, M. E. Light, *Organometallics* **2004**, *23*, 166–168.
[44] M. Gagliardo, P. A. Chase, S. Brouwer, G. P. M. van Klink, G. van Koten, *Organometallics* **2007**, *26*, 2219–2227.
[45] B. C. Gruver, J. J. Adams, S. J. Warner, N. Arulsamy, D. M. Roddick, *Organometallics* **2011**, *30*, 5133–5140.
[46] S. Tang, N. von Wolff, Y. Diskin-Posner, G. Leitus, Y. Ben-David, D. Milstein, *J. Am. Chem. Soc.* **2019**, *141*, 7554–7561.
[47] J. J. Adams, N. Arulsamy, D. M. Roddick, *Organometallics* **2011**, *30*, 697–711.
[48] S. Murugesan, K. Kirchner, *Dalt. Trans.* **2016**, *45*, 416–439.
[49] D. Spasyuk, S. Smith, D. G. Gusev, *Angew. Chemie* **2013**, *125*, 2598–2602.
[50] C. Liu, R. van Putten, P. O. Kulyaev, G. A. Filonenko, E. A. Pidko, *J. Catal.* **2018**, *363*, 136–143.
[51] K. Larmier, W.-C. Liao, S. Tada, E. Lam, R. Verel, A. Bansode, A. Urakawa, A. Comas-Vives, C. Copéret, *Angew. Chemie Int. Ed.* **2017**, *56*, 2318–2323.
[52] W.-H. Wang, Y. Himeda, J. T. Muckerman, G. F. Manbeck, E. Fujita, *Chem. Rev.* **2015**, *115*, 12936–12973.
[53] H. Yang, C. Zhang, P. Gao, H. Wang, X. Li, L. Zhong, W. Wei, Y. Sun, *Catal. Sci. Technol.* **2017**, *7*, 4580–4598.
[54] M. Andérez-Fernández, L. K. Vogt, S. Fischer, W. Zhou, H. Jiao, M. Garbe, S. Elangovan, K. Junge, H. Junge, R. Ludwig, M. Beller, *Angew. Chemie Int. Ed.* **2017**, *56*, 559–562.
[55] C. J. A. Daley, S. H. Bergens, *J. Am. Chem. Soc.* **2002**, *124*, 3680–3691.
[56] R. J. Hamilton, S. H. Bergens, *J. Am. Chem. Soc.* **2006**, *128*, 13700–13701.
[57] R. J. Hamilton, S. H. Bergens, *J. Am. Chem. Soc.* **2008**, *130*, 11979–11987.
[58] M. Zimmer-De Iuliis, R. H. Morris, *J. Am. Chem. Soc.* **2009**, *131*, 11263–11269.
[59] A. Passera, A. Mezzetti, *Adv. Synth. Catal.* **2019**, *361*, 4691–4706.
[60] A. Pham, J. Jarczyk, C. Reynolds, E. Kelly, S. Kim, T. He, T. Keith, J. Chianese, **2021**, DOI 10.26434/chemrxiv.13618988.v1.

[61] C. Bannwarth, E. Caldeweyher, S. Ehlert, A. Hansen, P. Pracht, J. Seibert, S. Spicher, S. Grimme, *WIREs Comput. Mol. Sci.* **2021**, *11*, DOI 10.1002/wcms.1493.
[62] C. Bannwarth, S. Ehlert, S. Grimme, *J. Chem. Theory Comput.* **2019**, *15*, 1652–1671.
[63] S. Grimme, C. Bannwarth, P. Shushkov, *J. Chem. Theory Comput.* **2017**, *13*, 1989–2009.
[64] Gaussian 16, Revision C.01, M. J. Frisch, G. W. Trucks, H. B. Schlegel, G. E. Scuseria, M. A. Robb, J. R. Cheeseman, G. Scalmani, V. Barone, G. A. Petersson, H. Nakatsuji, X. Li, M. Caricato, A. V Marenich, J. Bloino, B. G. Janesko, R. Gomperts, B. Mennucci, H. P. Hratchian, J. V. Ortiz, A. F. Izmaylov, J. L. Sonnenberg, D. Williams-Young, F. Ding, F. Lipparini, F. Egidi, J. Goings, B. Peng, A. Petrone, T. Henderson, D. Ranasinghe, V. G. Zakrzewski, J. Gao, N. Rega, G. Zheng, W. Liang, M. Hada, M. Ehara, K. Toyota, R. Fukuda, J. Hasegawa, M. Ishida, T. Nakajima, Y. Honda, O. Kitao, H. Nakai, T. Vreven, K. Throssell, J. A. Montgomery Jr., J. E. Peralta, F. Ogliaro, M. J. Bearpark, J. J. Heyd, E. N. Brothers, K. N. Kudin, V. N. Staroverov, T. A. Keith, R. Kobayashi, J. Normand, K. Raghavachari, A. P. Rendell, J. C. Burant, S. S. Iyengar, J. Tomasi, M. Cossi, J. M. Millam, M. Klene, C. Adamo, R. Cammi, J. W. Ochterski, R. L. Martin, K. Morokuma, O. Farkas, J. B. Foresman, D. J. Fox, Gaussian Inc., Wellingford CT, 2016..
[65] F. Weigend, R. Ahlrichs, *Phys. Chem. Chem. Phys.* **2005**, *7*, 3297.
[66] M. Bühl, H. Kabrede, *J. Chem. Theory Comput.* **2006**, *2*, 1282–1290.
[67] K. P. Jensen, B. O. Roos, U. Ryde, *J. Chem. Phys.* **2007**, *126*, 014103.
[68] A. V. Marenich, C. J. Cramer, D. G. Truhlar, *J. Phys. Chem. B* **2009**, *113*, 6378–6396.
[69] C. Adamo, V. Barone, *J. Chem. Phys.* **1999**, *110*, 6158–6170.
[70] A. D. Becke, *Phys. Rev. A* **1988**, *38*, 3098–3100.
[71] E. Caldeweyher, C. Bannwarth, S. Grimme, *J. Chem. Phys.* **2017**, *147*, 034112.
[72] A. V. Kalikadien, E. A. Pidko, V. Sinha, *Chemarxiv* **2021**, DOI 10.26434/chemrxiv.14617320.
[73] V. Sinha, J. J. Laan, E. A. Pidko, *Phys. Chem. Chem. Phys.* **2021**, *23*, 2557–2567.
[74] C. Hansch, A. Leo, R. W. Taft, *Chem. Rev.* **1991**, *91*, 165–195.

Manuscript received: March 3, 2021
Revised manuscript received: April 30, 2021
Accepted manuscript online: May 11, 2021

ARTICLE

A. M. Krieger, Dr. V. Sinha, A. V. Kalikadien, Prof. Dr. E. A. Pidko**